Journal of Structural Geology 31 (2009) 989–995

Contents lists available at ScienceDirect

Journal of Structural Geology

journal homepage: www.elsevier.com/locate/jsg

Discrete element modeling of the faulting in the sedimentary cover above an active salt diapir

Hongwei Yin*, Jie Zhang, Lingsen Meng, Yuping Liu, Shijing Xu

Department of Earth Sciences, Nanjing University, Nanjing 210093, China

ARTICLE INFO

Article history:
Received 15 April 2007
Received in revised form
31 July 2008
Accepted 16 October 2008
Available online 29 October 2008

Keywords:
Active salt doming
Discrete element model
Reitbrook dome
Radial normal faults

ABSTRACT

Geological mapping, seismic analyses, and analogue experiments show that active salt diapirism results in significant faulting in the overburden strata. Faults associated with active diapirism generally develop over the crest of the dome and form a radial pattern. In this study, we have created a 3-D discrete element model and used this model to investigate the fault system over active diapirs. The model reproduces some common features observed in physical experiments and natural examples. The discrete element results show that most faults initiate near the model surface and have displacement decreasing downward. In addition, model results indicate that the earliest fault, working as the master fault, has a strong influence on the subsequent fault pattern. The footwall of the master fault is mainly deformed by arc-parallel stretching and develops a subradial fault pattern, whereas the hanging wall is deformed by both arc-parallel stretching and gliding along the master fault and top of salt, and hence develops both parallel and oblique faults. Model results replicate the fault pattern and deformation mechanism of the Reitbrook dome, Germany.

1. Introduction

An active diapir forcefully intrudes its overburden, driven by diapir pressure that overcomes the resistance of the overburden strength (Schultz-Ela et al., 1993). Active diapirs are generally circular or elliptical in map view. Most sedimentary rocks above active diapirs are heavily deformed by faulting and folding (Withjack and Scheiner, 1982; Schultz-Ela et al., 1993; Davison et al., 2000a, 2000b; Yin and Groshong, 2006, 2007). Although the geometries of faults associated with active salt diapirs are highly complex, they share several characteristic features. The faults associated with active salt doming are normal and commonly form a radial pattern in the map view.

Although investigations by geologists have illustrated the common features of faults associated with active salt diapirs, our understanding of the fault development is far from complete. The fault patterns in the brittle cover over active domes are typically complex because of the strongly 3-D nature of the deformation around the circular to elliptical structures. Surface exposures are rare, and our knowledge of active salt domes is obtained primarily from physical experiments, numerical modeling, and subsurface data. Most physical experiments are observed in cross section. While structural styles observed in the map view (e.g., Parker and McDowell, 1951; Withjack and Scheiner, 1982; Alsop, 1996; Yamada et al., 2005) or cross section (Cloos, 1955; Currie, 1956; Brewer and Groshong, 1993; Schultz-Ela et al., 1993) have significantly expanded our knowledge of the fault patterns of active salt domes, this 2-D technique has limitations when applied to define the 3-D fault patterns. In the absence of satisfactory understanding of 3-D fault patterns, interpretations based on well logs and seismic data are challenging because the strata are heavily faulted, making the correlation of fault very difficult. Numerical modeling is another approach to investigate active salt diapirism. Several investigators have used a finite element method to investigate active diapirism (e.g., Daudre and Cloetingh, 1994; Mazariegos et al., 1996). However, this continuum technique was mainly used to study the mechanism of active intrusion, and rarely to investigate the 3-D structural patterns of the faults over the intrusion.

To better understand the 3-D structural pattern and evolution of faults over active salt diapir, we have created a 3-D discrete element model. The discrete element technique (Cundall and Strack, 1979; Mora and Place, 1993, 1994; Place et al., 2002) is based on molecular dynamics, well established in the fields of physics and fluid dynamics. Unlike continuum techniques, this method permits large relative motion inside the model and simulates its evolution dynamically. It is a technique well suited to investigate heavily faulted structures. In recent years, investigators have used this technique to study a number of geological and

* Corresponding author. Tel.: +86 25 83686759; fax: +86 25 83596016.
E-mail address: hwyin@nju.edu.cn (H. Yin).

0191-8141/$ – see front matter © 2008 Elsevier Ltd. All rights reserved.
doi:10.1016/j.jsg.2008.10.007

geophysical problems, such as the reactivation of basement faults (Saltzer and Pollard, 1992), compressional folding and orogenic evolution (Morgan, 1997; Morgan and McGovern, 2005; Burbridge and Braun, 2002; Vietor, 2003; Strayer et al., 2004), fault propagation folding (Finch et al., 2003; Hardy and Finch, 2006, 2007), and graben formation (Seyferth and Henk, 2003). In this study, we use the discrete element technique to investigate the deformation over active diapirs, particularly the initiation and evolution of the faults.

2. 3-D discrete element model

2.1. Method

The discrete element model used here is developed from the lattice solid model (Mora and Place,1993, 1994; Place et al., 2002). The model elements consist of a series of soft spheres which obey Newton's equations of motion. The elements interact in pairs as if connected by breakable elastic springs and undergo motion relative to one another. The behavior of the elements assumes that the particles interact through a "repulsive–attractive" force (Mora and Place, 1993) in which the force Fs is given as:

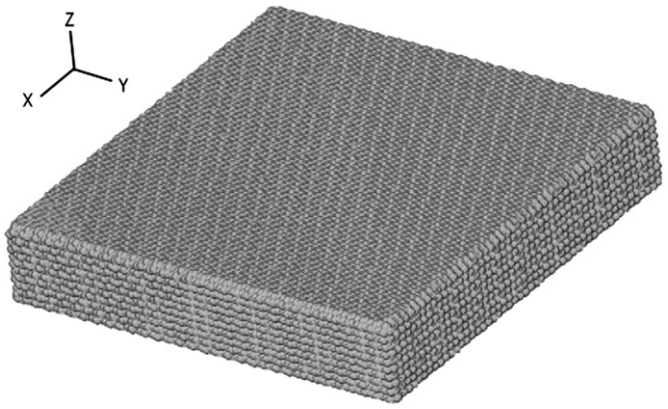

Fig. 1. Set-up of discrete element model. The discrete element model is composed of a regular hexagonal, homogenous lattice of 170,150 spheres with radius of one unit, represent the brittle sedimentary cover. The model is initially 170 units long, 170 units wide, and 30 units thick. Each unit represents 10 m.

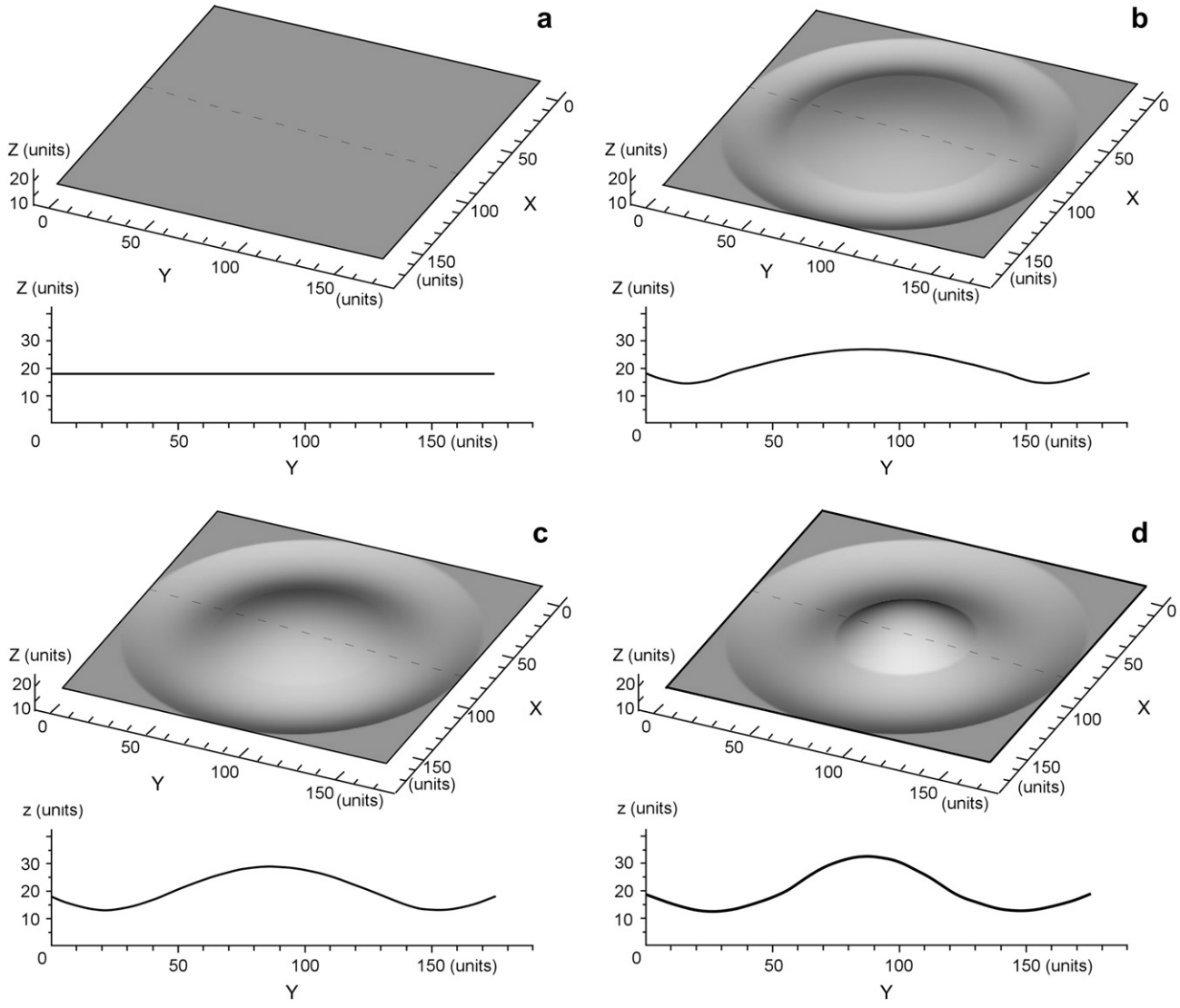

Fig. 2. The basal boundary of the model. (a) The horizontal basal boundary before deformation. (b) The basal boundary in the early stage of active doming. (c) The basal boundary in the middle stage of active doming. (d) The basal boundary in the late stage of active doming. The dashed line on the map shows the location of the cross section.

$$\mathrm{Fs} = \begin{cases} K(r-R), & r < r_0, \text{ intact bond} \\ K(r-R), & r < R, \text{ broken bond} \\ 0, & r >= R, \text{ broken bond} \end{cases} \quad (1)$$

where K is the spring strength of the relative bond, R is the equilibrium separation between the particles, r_0 is a defined breaking separation, and r is the separation between the particle pairs. Particles are bonded to their neighbors, and experience an attractive or repulsive force calculated by the equation above from adjacent particles. Once the distance between the two neighbors exceeds r_0, the spring is broken and no more attractive force will exist between the old neighbors. However, if the two particles return to a compressive contact (i.e., $r < R$), a repulsive force acts between them. Mora and Place (1994) tested the parameters and showed that breaking strains for most materials are typically much less than 0.11. Finch et al. (2003) investigated the effect of smaller and larger values of the breaking separation and showed that large values of the breaking strain produce "strong" materials which fail by localized faulting, whereas low values produce "weak" materials which deform in a macroscopically ductile manner. The total elastic force exerted on a particle is obtained by summing the forces on each bond that links the particle to its neighbors. In addition, the model includes the effect of gravitational forces and a viscous damping term (cf. Mora and Place, 1994; Place et al., 2002; Finch et al., 2003). At each time step, elements move to their new positions. The model calculates the position of elements by integrating equations of motion using Newtonian physics (cf. Mora and Place, 1994; Place et al., 2002; Finch et al., 2003).

2.2. Boundary conditions and experimental parameters

In this study we apply the discrete element model to investigate the fault system over an active salt diapir, in which a brittle sedimentary cover is faulted and folded in response to the salt upward movement. We use a regular hexagonal, homogenous lattice of 170,150 spheres with radius of one unit to represent the brittle sedimentary cover. The model is initially 170 units long, 170 units wide, and 30 units thick (Fig. 1). Here, we focus on the deformation of the brittle sedimentary cover, and do not include the salt body in the model. The model has four fixed side boundaries and a changing basal boundary. Before deformation, the basal boundary is horizontal (Fig. 2a). As doming begins, the basal boundary changes to a radially symmetric curved surface, consisting of a pillow and a periphery low (Fig. 2b). With continuing deformation, the pillow gets narrower and higher; simultaneously, the periphery low sink zone becomes broader and deeper (Fig. 2c,d). Given the position of the pillow crest, we describe the curved surface (i.e., the basal boundary) using a trigonometric function. This changing basal boundary is an approximation of the salt top proposed by Trusheim (1960).

In this study, one lattice unit corresponds to 10 m, appropriate for the scale of deformation associated with active diapirs, and rock density is defined as 2.5 g cm^{-3}, typical of upper-crustal sedimentary rocks. We use a value of the spring constant, K of 5.2×10^9 N m^{-1}, and a value of the breaking strain of 0.02. These values are chosen as a result of trial and error. We ran the model repeatedly to find the values that are appropriate (i.e., no significant gaps and cliffs form as a result of improper choosing of material strength under the influence of normal gravity). The value of the spring constant in the model presented here implies that the equivalent value of Young's modulus is approximately 5 GPa. Like other discrete-element techniques that are derived from the lattice solid model of Mora and Place (1993, 1994) (e.g., Strayer et al., 2004; Hardy and Finch, 2005), the appropriate values of Young's modulus are an order of magnitude smaller than laboratory experiments on rock samples. One reason might be that the natural systems involving larger volumes of rock contain more joints and small faults, and thus Young's modulus decreases with increasing sample size (Bieniawski, 1984).

The model ran for a total of 800,000 time steps. At each time step, the crest of the dome moved upward 0.0000173 units, resulting in a total uplift of about 14 units (138.4 m). A complete model run takes 140 h CPU time of a 4-node cluster which has a peak performance of about 20 Gflops.

3. Experimental results

3.1. Fault formation and evolution

In the early stage of the model, the cover was arched with distributed fractures developing on the surface. However, obvious faulting with more than two units (20 m) slip did not occur until 500,000 time steps (86.5 m uplift) (Fig. 3). This first fault initiated near the crest of the fold, and propagated on both sides on strike and downward.

After 650,000 time steps (112.5 m uplift), fault 1 propagated and soled into the top of salt, and also six new faults were observed (Fig. 4). Fault 2, fault 3, and fault 7 developed on the footwall of fault 1, and they were roughly perpendicular to fault 1. The other new fault on the footwall is fault 4, which is near the dome crest, parallel to and dipping away from fault 1. Fault 5 developed on the hanging wall of fault 1, parallel to and dipping toward fault 1. Fault 6 offset fault 1 and deformed both the hanging wall and footwall of fault 1. Five of the six new faults initiated near the top of the model, and propagated downward, except fault 5, which initiated near the top of salt, and propagated upward. By 650,000 time steps (112.5 m uplift), this fault had not reached the surface of the model. Fault 1 is the largest fault with a maximum slip of about three units (30 m). The maximum slip of other faults is about two units (20 m).

With 800,000 time steps (138.4 m uplift), fault 5 propagated to the surface of the model, and all the downward propagating faults reached the salt top. The maximum slip of fault 1 had reached four units (40 m). From 650,000 to 800,000 time steps, only one new

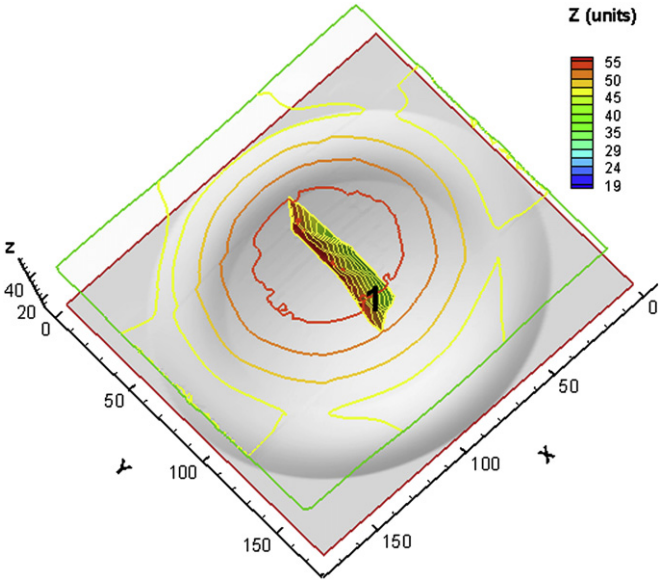

Fig. 3. Model results after 500,000 time steps (86.5 m uplift). The top of salt is shown as a shaded surface. The top of the model is represented by contour lines. The colored plane is the fault.

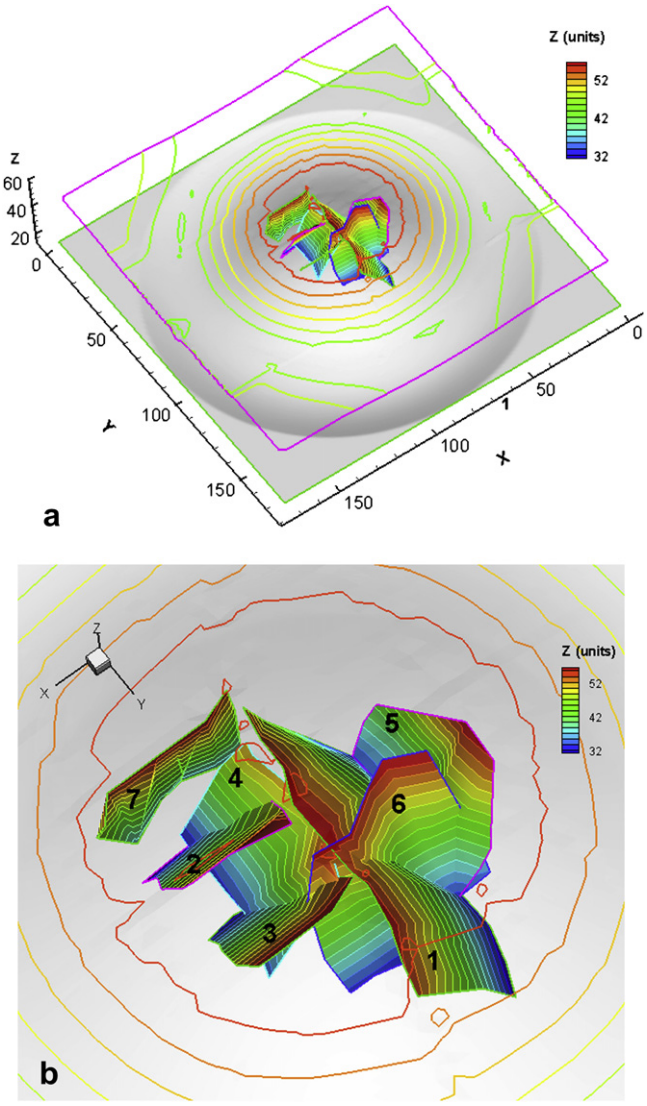

Fig. 4. Model results after 650,000 time steps (112.5 m uplift). The top of salt is shown as a shaded surface. The top of the model is represented by contour lines. The colored planes are faults. (a) 3-D view of the model. (b) Fault pattern in 3-D.

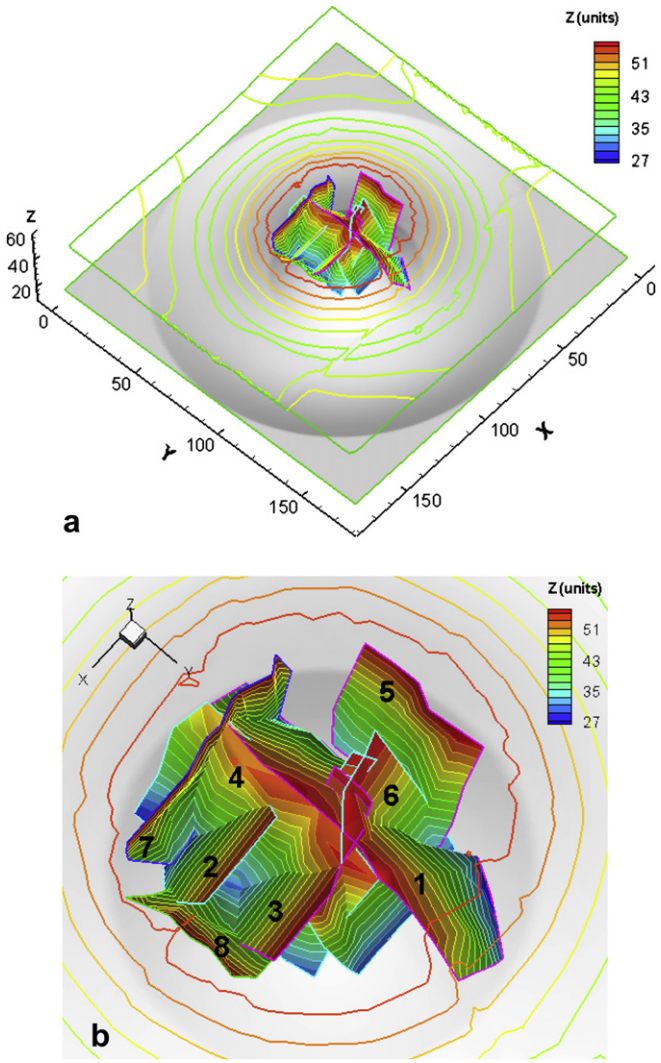

Fig. 5. Model results after 800,000 time steps (138.4 m uplift). The top of salt is shown as a shaded surface. The top of the model is represented by contour lines. The colored planes are faults. (a) 3-D view of the model. (b) Fault pattern in 3-D.

fault formed in the footwall of the fault 1. This fault, fault 8, initiated near the top of salt and propagated upward. The hanging wall of fault 1 developed two antithetic faults, fault 9 and 10. Two upward propagating faults, 5 and 8, form the boundaries of the faulted region. Within the region, the cover was heavily fractured and faulted, whereas out of the region, the cover was deformed by block rotation and flexural slip, no obvious fault is observed (Figs. 6, 7).

3.2. Structural styles in cross section and map

Map and cross sections show that faults are limited to the arched area of the cover (Figs. 6, 7). Faults 5 and 8 have maximum displacement near the bottom of the model. They might have been influenced by high curvature along the shoulders of the dome in this region. Whereas, faults 1, 2, 3, 4, 6, 7 have displacements that decrease downward. They initiated near the model surface and are created by the arc-parallel extension. Cross sections also show that for highly 3-D structures, the structural geometries observed in 2-D depend on the location and orientation of the profile. The structural style in the cross section could appear as a full graben (Fig. 6a), a half graben with an anti-listric boundary fault (Fig. 6b), a half graben with planar boundary fault (Fig. 6c), and domino half grabens (Fig. 6d). On the surface map (Fig. 7), it can be seen that the earliest fault, fault 1, cuts the arched region into two blocks. The footwall shows a subradial fault pattern with 3 faults (faults 2, 3, and 7) perpendicular to the master fault, whereas the hanging wall has one normal fault oblique to the master fault and two secondary antithetic normal faults that are approximately parallel to the master fault. Faults 5 and 8 are close to the margin of the arched region. As described above, these two faults initiated near the bottom of the model and propagated upward. Only a small part of these two faults reached the surface after 800,000 model time steps (138.4 m uplift).

4. Discussion

A radial normal fault pattern is one of the characteristic features of natural and experimental active salt diapirs. In our discrete element experiments, no typical radial fault pattern appears. Instead, faults have two principal trends approximately parallel to the model margin (Figs. 5, 7). Two important factors that may

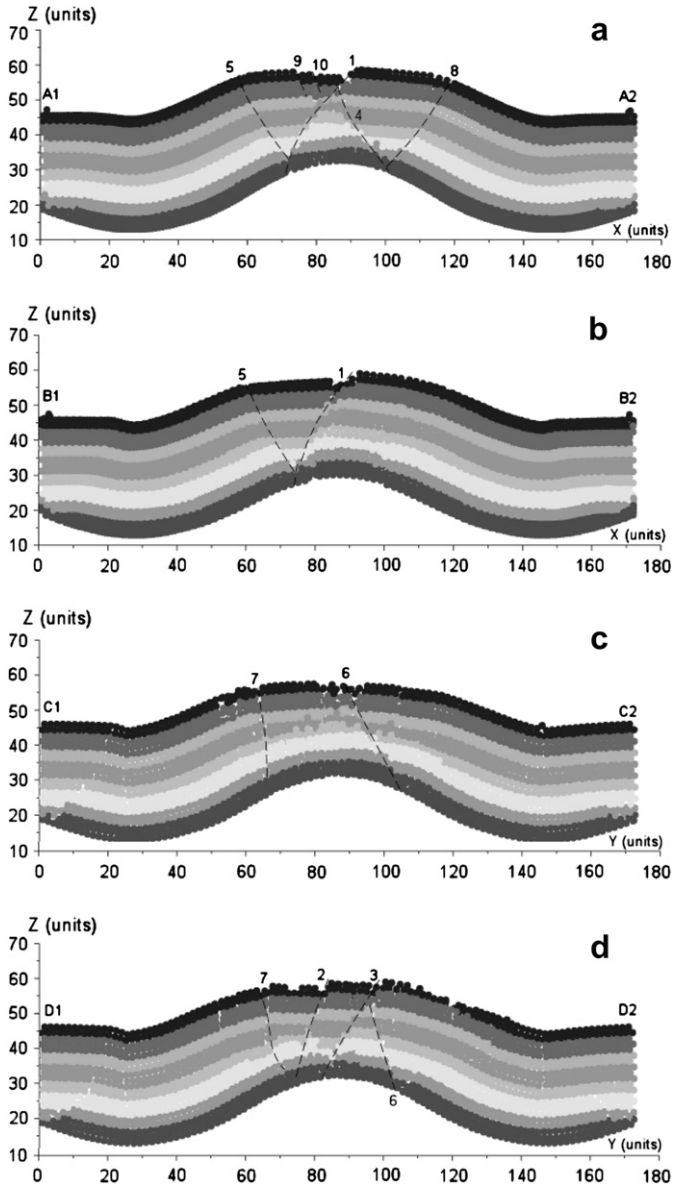

Fig. 6. Cross sections cut from the model after 800,000 time steps (see Fig. 7 for locations). (a) Cross section perpendicular to the earliest fault (fault 1) and near the center of the dome. (b) Cross section perpendicular to the earliest fault and off the center of the dome. (c) Cross section parallel to the earliest fault and across its hanging wall. (d) Cross section parallel to the earliest fault and across its footwall.

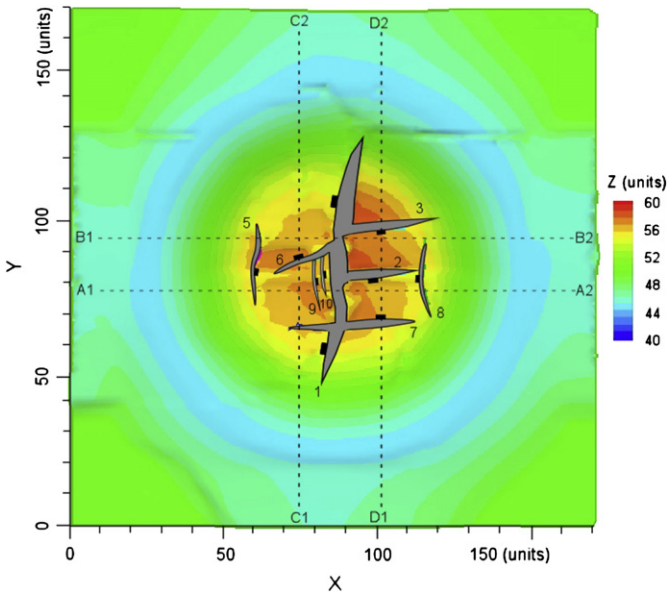

Fig. 7. Map of the model surface after 800,000 time steps.

influence the fault pattern of the model are boundary conditions and the lattice arrangement of the particles.

The basal boundary is radially symmetric. Theoretically, it will not intrigue faults paralleled to the axes. To test the influence of side boundaries on the fault orientation, we changed the side boundary to be a cylinder wall. However, the main fault pattern remained. It seems that the side wall boundaries do not contribute to the fault distribution pattern. Alternatively, the lattice arrangement of the particles may have influenced the fault orientations. The lattice is arranged by hexagonal closest packing with rows of particles parallel to the *x* axis. This lattice arrangement may have resulted in preferred cleavage directions, and hence influences the orientations of the faults in the model.

The numerical results described above are comparable to an active salt diaper that has one or two master faults which cross the arched region, such as the Reitbrook dome, Germany (Fig. 8).

The Reitbrook dome is one of the best documented active salt domes in the world with 265 wells drilled since 1937 (Schmitz and Flixeder, 1993). Early maps and cross sections were published by Behrmann (1949). Behrmann (1949) interpreted the Reitbrook dome as a salt diapir with a series of approximately parallel normal faults, which was thought to be due to regional extension. Since then, the Reitbrook dome has been cited often as a model for a fault pattern above a rising salt diaper under horizontal extension (e.g., Gussow, 1968; Mandl, 1988). Schmitz and Flixeder (1993) did a detailed structural analysis using many wells in the oil field and interpreted the Reitdome as a circule dome with no significant horizontal stress field. The interpretation by Schmitz and Flixeder (1993) shows a master fault that crosses the arched region along the NE direction. The footwall of the master fault has a radial fault pattern, whereas the hanging wall of the master fault develops parallel, oblique, and radial faults. There is a clear and interesting correlation between the mapped fault geometries of the discrete element model (Fig. 7) and the Reitbrook dome interpreted by Schmitz and Flixeder (1993) (Fig. 8). They both have a master fault (fault 1) that crosses over the arched region. Based on the results from the discrete model, the master fault is the earliest and largest fault, and has a strong influence on the subsequent deformation of the dome. The footwall of the master is primarily deformed by block rotation and arc-parallel stretching, and is dominated by faults approximately perpendicular to the master fault. The hanging wall has a strong influence from the slip along the master fault and the top of the salt, and hence produces both oblique and parallel secondary faults. One big difference between the model and the Reitbrook dome is size of the graben developed near the crest of the dome. The Reitbrook dome has a big graben bounded by the through-going master fault and one large antithetic fault (Fig. 8). However, the model develops a small size graben, which is bounded by the master fault and deformed by a series of small antithetic faults (Figs. 6a, 7). Horizontal stress might be the cause of the difference. The side boundary walls of our model are fixed. The Reitbrook dome, however, might have experienced some regional extension, especially during the early stage of the dome growth. Instead of being a significant regional extension as suggested by Behrmann (1949), the extension during the Reitbrook dome growth could be very slight, and hence is not indicated by the field data analysis

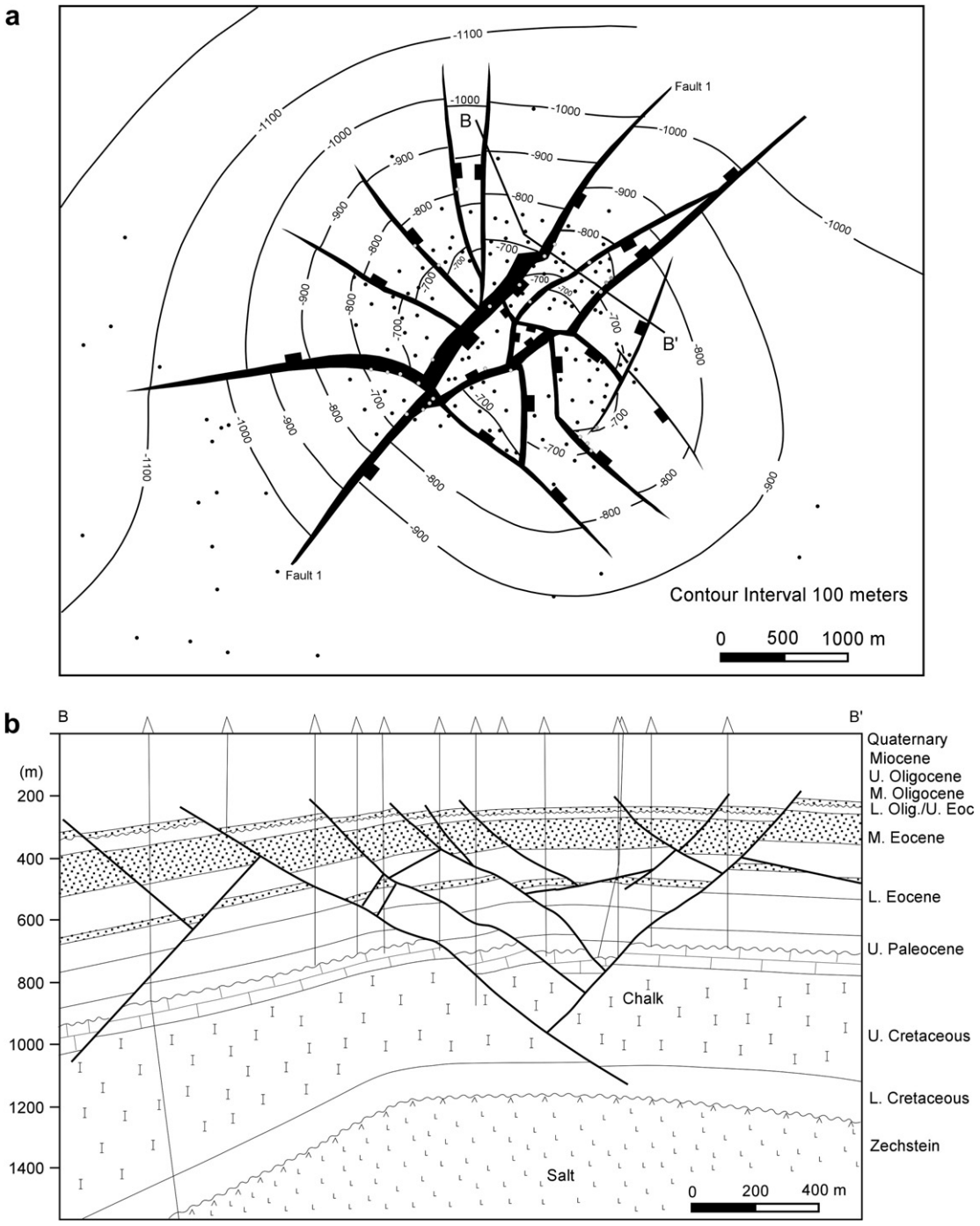

Fig. 8. The Reitbrook dome (after Schmitz and Flixeder, 1993). (a) The structure contour map drawn on the base of the Tertiary in Reitbrook dome, Northern Germany. (b) Cross section drawn perpendicular to the master fault.

(Schmitz and Flixeder, 1993) and map view restoration (Yin and Groshong, 2006).

5. Conclusion

A 3D discrete element model has been developed to investigate the deformation of the cap-rock above a rising salt dome. The model reproduces some common features seen in physical experiments and reported natural examples. Our experimental results show that active salt doming resulted in numerous normal faults in the cover. Most of the faults initiate near the model surface and have displacement decreasing downward, except the two faults near the margin of the arched region, which initiate near the model bottom and have displacement increasing downward. In addition, our model results indicate that the earliest fault works as the master fault and has a great influence on the subsequent fault pattern. The footwall of the master fault is mainly deformed by arc-parallel stretching and hence develops a subradial fault pattern, while the hanging wall is deformed by both arc-parallel stretching and gliding along the master fault, and so develops both parallel and oblique faults.

Acknowledgements

This research has been supported the National Natural Science Foundation of China Contract No. 40402019. Comments and

suggestions from Julia Morgan, Martha O. Withjack and the volume editor Terry Engelder have greatly improved this manuscript. Thanks must also go to Huiqun Zhou of the Nanjing University for his support during the development of the discerte element code. This paper is dedicated to Rick Groshong. As Dr Groshong's PhD student, Hongwei Yin sincerely thanks Rick for his guidance and support. Dr Groshong's enthusiasm for scientific research in structural geology has had a lasting influence on me since my PhD study at the University of Alabama.

References

Alsop, G.I., 1996. Physical modelling of fold and fracture geometries associated with salt diapirism. In: Alsop, G.I., Brundell, D.J., Davison, I. (Eds.), Salt Tectonics. Geological Society, London, Special Publication, vol. 100, pp. 227–241.

Behrmann, R.B., 1949. Geologie und lagerstatte desOelfeldes Reitbrook bei Hamburg. In: Bentz, A. (Ed.), Erdoel und Tektonik in Nordeswestdeutschland: Hannover, Sammelband, pp. 190–221.

Bieniawski, Z.T., 1984. Rock Mechanics Design and Tunnelling. Balkema.

Brewer, R.C., Groshong Jr., R.H., 1993. Restoration of cross sections above intrusive salt domes. AAPG Bulletin 77, 1769–1780.

Burbridge, D.R., Braun, J., 2002. Numerical models of the evolution of accretionary wedges and fold-and-thrust belts using the distinct element method. Geophysical Journal International 148, 542–561.

Cloos, E., 1955. Experimental analysis of fracture patterns. GSA Bulletin 66, 241–256.

Cundall, P.A., Strack, O.D.L., 1979. A discrete numerical model for granular assemblies. Geotechnique 29, 47–65.

Currie, J.B., 1956. Role of concurrent deposition and deformation of sediments in development of salt-dome graben structures. American Association of Petroleum Geologists Bulletin 40, 1–16.

Daudre, B., Cloetingh, S., 1994. Numerical modeling of salt diapirism: influence of the tectonic regime. Tectonophysics 240, 59–79.

Davison, I., Alsop, I., Birch, P., Elders, C., Evans, N., Nicholson, H., Rorison, P., Wade, D., Woodward, J., Young, M., 2000a. Geometry and late-stage structural evolution of Central Graben salt diapirs, North Sea. Marine and Petroleum Geology 17, 499–522.

Davison, I., Alsop, I., Evans, N.G., Safaricz, M., 2000b. Overburden deformation patterns and mechanisms of salt diaper penetration in the Central Graben, North Sea. Marine and Petroleum Geology 17, 601–618.

Finch, E., Hardy, S., Gawthorpe, R., 2003. Discrete element modeling of contractional fault propagation folding above rigid basement fault blocks. Journal of Structural Geology 25, 515–528.

Gussow, W.C., 1968. Salt diapirism: importance of temperature, and energy source of emplacement. In: Braunstein, J., O'Brien, G.D. (Eds.), Diapirism and Diapirs. AAPG Memoir, 8, pp. 16–52.

Hardy, S., Finch, E., 2005. Discrete-element modelling of detachment folding. Basin Research 17, 507–520.

Hardy, S., Finch, E., 2006. Discrete element modeling of the influence of cover strength on basement-involved fault-propagation folding. Tectonophysics 415, 225–238.

Hardy, S., Finch, E., 2007. Mechanical stratigraphy and the transition from trishear to kink-band fault-propagation fold forms above blind basement thrust faults: a discrete-element study. Marine and Petroleum Geology 24, 75–90.

Mandl, G., 1988. Mechanics of Tectonic Faulting: Models and Basic Concepts. Elsevier, Amsterdam, pp. 1-407.

Mazariegos, R.A., Andrews, M.J., Russell, J.E., 1996. Modeling of evolution of salt structures using nonlinear rocksalt flow laws. Tectonophysics 256, 129–143.

Mora, P., Place, D., 1993. A lattice solid model for the non-linear dynamics of earthquakes. International Journal of Modern Physics C4, 1059–1074.

Mora, P., Place, C., 1994. Simulation of the frictional stick-slip instability. Pure and Applied Geophysics 143, 61–87.

Morgan, J.K., 1997. Studying submarine accretionary prisms in a "numerical sandbox": simulations using the distinct element method. Eos Transaction of the AGU, Fall Meeting (Suppl.) 78, F707.

Morgan, J.K., McGovern, P.J., 2005. Discrete element simulations of gravitational volcanic deformation: 1. Deformation structures and geometries. Journal of Geophysical Research 110, B05402.

Place, D., Lombard, F., Mora, P., Abe, S., 2002. Simulation of the micro-physics of rocks using LSMEarth. Pure and Applied Geophysics 159, 1911–1932.

Parker, T.J., McDowell, A.N., 1951. Scale model as guide to interpretation of salt dome faulting. AAPG Bulletin 35, 2076–2086.

Saltzer, S.D., Pollard, D.D., 1992. Distinct element modeling of structures formed in sedimentary overburden by extensional reactivation of basement normal faults. Tectonics 11, 165–174.

Schmitz, J., Flixeder, F., 1993. Structure of a classic chalk oil field and production enhancement by horizontal drilling, Reitbrook, NW Germany. In: Spencer, A.M. (Ed.), Generation, Accumulation and Production of Europe's Hydrocarbons III. European Association of Petroleum Geoscientists Special Publication 3, pp. 144–154.

Schultz-Ela, D.D., Jackson, M.P.A., Vendeville, B.C., 1993. Mechanics of active salt diapirism. Tectonophysics 228, 275–312.

Seyferth, M., Henk, A., 2003. Coupling the PFC2D and ANSYS – concepts to combine the best of two worlds for improved geodynamic models. In: Konietzky, H. (Ed.), Numerical Modeling in Micromechanics via Particle Methods, pp. 283–290.

Strayer, L.M., Erickson, S.G., Suppe, J., 2004. Influence of growth strata on the evolution of fault-related folds: distinct element models. In: McClay, K.R. (Ed.), Thrust Tectonics. AAPG Memoir, 82, pp. 413–437.

Trusheim, F., 1960. Mechanism of salt migration in northern Germany. AAPG Bulletin 44, 1519–1540.

Vietor, T., 2003. Numerical simulation of collisional orogeny using the distinct element technique. In: Konietzky, H. (Ed.), Numerical Modeling in Micromechanics via Particle Methods, pp. 295–301.

Withjack, M.O., Scheiner, C., 1982. Fault patterns associated with domes-an experimental and analytical study. AAPG Bulletin 66, 302–316.

Yamada, Y., Okamura, H., Tamura, Y., Tsuneyama, F., 2005. Analog models of faults associated with salt doming and wrenching: application to offshore United Arab Emirates. In: Sorkhabi, R., Tsuji, Y. (Eds.), Faults, Fluid Flow, and Petroleum Traps. AAPG Memoir, 85, pp. 95–106.

Yin, H., Groshong Jr., R.H., 2006. Balancing and restoration of piercement structures: geologic insights from 3D kinematic models. Journal of Structural Geology 28, 99–114.

Yin, H., Groshong Jr., R.H., 2007. A three-dimensional kinematic model for the deformation above an active diaper. AAPG Bulletin 91, 343–363.